NANO LETTERS

pubs.acs.org/NanoLett Letter

Switchable Induced-Transmission Filters Enabled by Vanadium Dioxide

Chenghao Wan,[⊥] David Woolf,[⊥] Colin M. Hessel, Jad Salman, Yuzhe Xiao, Chunhui Yao, Albert Wright, Joel M. Hensley, and Mikhail A. Kats*

Cite This: *Nano Lett.* 2022, 22, 6−13 Read Online

ACCESS | Metrics & More | Article Recommendations | Supporting Information

ABSTRACT: An induced-transmission filter (ITF) uses an ultrathin metallic layer positioned at an electric-field node within a dielectric thin-film bandpass filter to select one transmission band while suppressing other bands that would have been present without the metal layer. We introduce a switchable mid-infrared ITF where the metal can be "switched on and off", enabling the modulation of the filter response from a single band to multiband. The switching is enabled by the reversible insulator-to-metal phase transition of a subwavelength film of vanadium dioxide (VO_2). Our work generalizes the ITF—a niche type of bandpass filter—into a new class of tunable devices. Furthermore, our fabrication process—which begins with thin-film VO_2 on a suspended membrane—enables the integration of VO_2 into any thin-film assembly that is compatible with physical vapor deposition processes and is thus a new platform for realizing tunable thin-film filters.

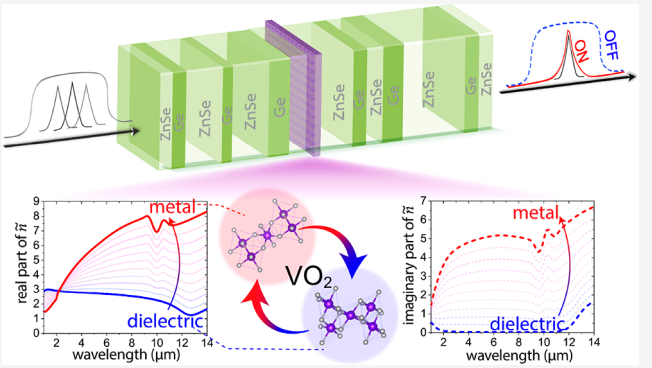

KEYWORDS: *phase-change materials, VO_2, thin-film filters, tunable filters*

INTRODUCTION

Various approaches have been employed to make optical filters tunable with respect to parameters such as wavelength, bandwidth, and transmission magnitude. Examples such as mechanically driven filter wheels,[1] tunable fiber Bragg gratings,[2,3] tunable Fabry−Pérot (F−P) resonators,[4,5] acousto-optic tunable filters,[6,7] and liquid-crystal tunable filters[8,9] have resulted in revolutionary developments in applications from optical communications[10] to detection and imaging.[11,12] More recently, efforts to create fast, compact, and tunable filters have focused on incorporating active media into either multilayer-[13−16] or metasurface-type[17−20] structures. Each of these two general approaches has different advantages and disadvantages; for example, metasurface-based designs are much thinner, are potentially much faster, and require fewer fabrication steps but are difficult to fabricate over the millimeter scale, whereas multilayer structures require no nanopatterning and thus scale more easily to larger areas.

Active materials that have been investigated for tunable filters include correlated transition-metal oxides,[21] germanium−antimony−tellurium (GST),[22] and gate-tunable graphene,[23] all of which have complex refractive indices that can be tuned via one or more external stimuli, such as thermal biasing, electrical gating, incident light, and strain.[24−26] In particular, thin-film VO_2 has been widely explored for tunable optical devices, especially in the mid- and far-infrared where it features a high refractive-index contrast and relatively low loss in one of its phases.[27] However, the integration of VO_2 into thin-film assemblies is challenging because of the high temperatures required to obtain the correct crystallographic state (typically, >500 °C[28−30]) and the dependence of its electrical and optical properties on the substrate and synthesis methods.[27,31]

In this paper, we proposed an alternative procedure—deposition of dielectric layers on both sides of an as-grown VO_2 on a Si membrane—to fabricate thin-film stacks comprising mid-infrared-transparent dielectric materials and VO_2, enabling the creation of tunable mid-infrared filters. We designed and fabricated an induced-transmission filter (ITF)—a dielectric thin-film filter that uses an ultrathin metal layer to remove unwanted sidebands around a desired passband—where the metal layer is replaced by VO_2. We designed filters with one or more tunable passbands and experimentally demonstrated a filter that switches between broadband

Received: June 13, 2021
Revised: December 14, 2021
Published: December 27, 2021

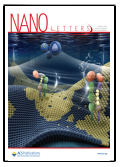

https://doi.org/10.1021/acs.nanolett.1c02296
Nano Lett. 2022, 22, 6−13

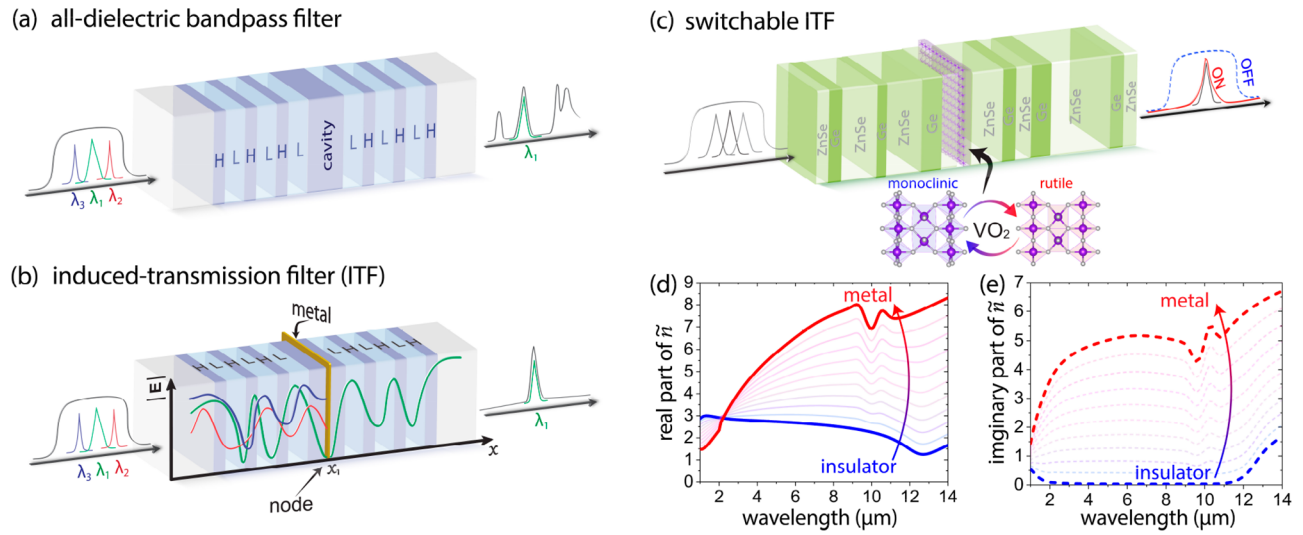

Figure 1. (a) Schematic of an all-dielectric single-cavity (Fabry−Perot-type) filter, with a high-index cavity sandwiched by alternating high-index (H) and low-index (L) dielectric films. This dielectric filter features a narrow transmission band but is accompanied by (usually unwanted) side bands at both shorter and longer wavelengths. (b) Schematic of a classic induced-transmission filter (ITF) in which an ultrathin metallic layer is introduced into the cavity at the position where the electric-field magnitude of the desired passband wavelength ($|E(\lambda_1)|$) is minimized, suppressing the unwanted sidebands. The schematics in (a, b) are rendered based on the design in ref.[33] (c) A schematic of our switchable ITF that features a broad transmission band (OFF state) when VO_2 is in the insulating phase and a narrow transmission band (ON state) when VO_2 is in the metallic phase. **(d, e)** The evolution of the complex refractive index of a VO_2 film across its insulator-to-metal transition (IMT).[27]

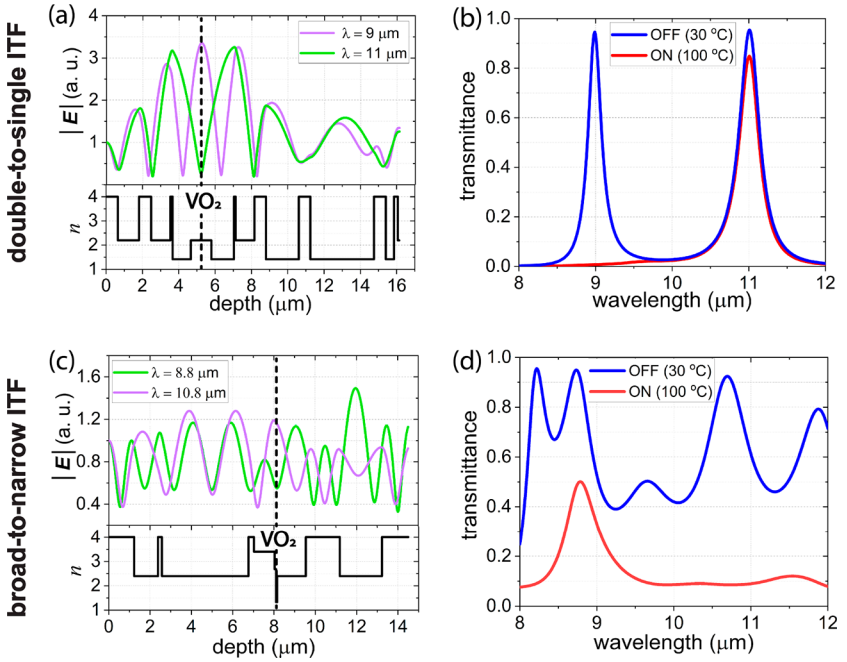

Figure 2. (a) Electric field distribution ($|E|$) in the dual-to-single bandpass ITF at wavelengths of 9 and 11 μm, when the VO_2 is in its insulating state. (b) Simulated OFF- and ON-state transmittance of the dual-to-single bandpass ITF. (c) Electric field distribution ($|E|$) in the broad-to-narrow bandpass filter at wavelengths of 8.8 and 10.8 μm, when the VO_2 is in its insulating state. (d) Simulated OFF- and ON-state transmittance of the broad-to-narrow bandpass ITF.

transmission in the long-wave infrared (LWIR, 8−12 μm) and a narrow passband around 8.8 μm.

DESIGN AND SIMULATION

Our design is inspired by the induced-transmission filter (ITF) proposed by Berning and Turner in 1957.[32] Their intent was to improve rejection of out-of-band transmission by introducing a thin metallic film into a narrow-bandpass filter comprising dielectric thin films.[32] For example, Figure 1a is a schematic of a conventional single-cavity all-dielectric filter[33] with a passband at free-space wavelength λ_1 but accompanied by unwanted side bands. If an ultrathin ($\ll\lambda_1$) metal is inserted at the position x_1 where the field is minimized (i.e., $|E(x_1, \lambda_1)| \sim 0$) (Figure 1b), the metallic film will have a minimum influence on $E(\lambda_1)$ everywhere. However, the electric field at the other wavelengths can be greatly affected by this metallic film, resulting in suppression of the sideband transmission.

https://doi.org/10.1021/acs.nanolett.1c02296
Nano Lett. 2022, 22, 6−13

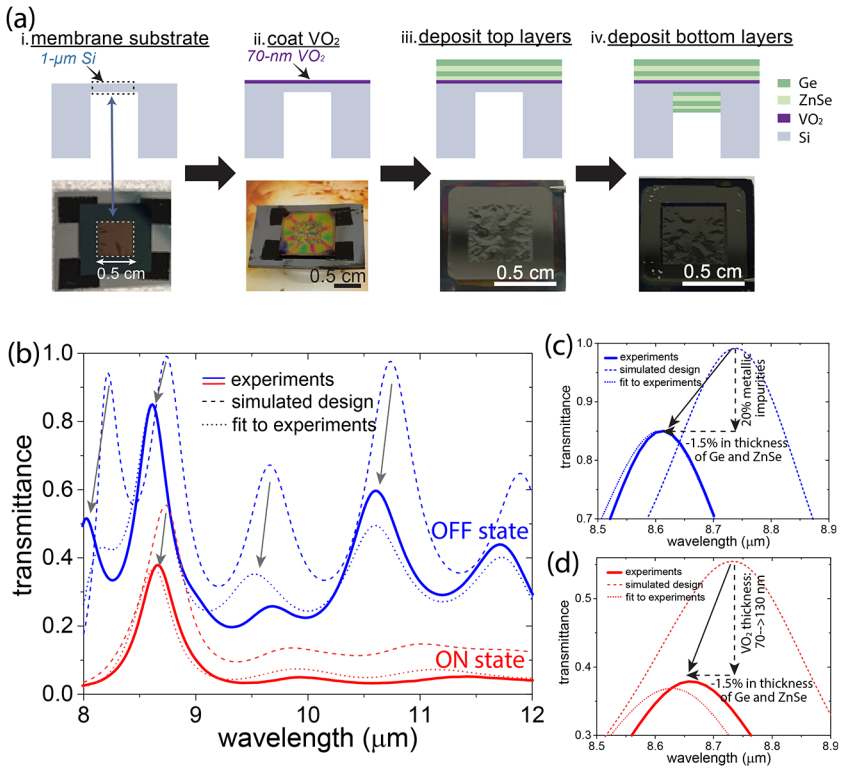

Figure 3. (a) Fabrication process. First, a VO_2 layer (target thickness = 70 nm; actual value ∼130 nm) was formed using the sol−gel method on the top side of a 1 μm thick Si membrane (5 × 5 mm) using the sol−gel method. Then, the ZnSe/Ge layers were deposited on the top and bottom sides of the sample, with the target thicknesses according to our simulation shown in Figure 2c. (b) FTIR transmittance measurements of the fabricated ITF for both OFF (at 30 °C) and ON states (at 100 °C). The dashed lines are calculation results, the same as those in Figure 2d. (c, d) Zoomed-in figures of "b" to better show the mechanisms that likely caused the reduction in transmittance and spectral shifts in our experiments.

This configuration is an ITF with a single narrow passband at λ_1.

ITFs have long since been supplanted by advanced multilayer dielectric thin-film coatings,[34] but recent research into phase-transition materials presents an opportunity for tunable devices. Directly replacing the metal layer in an ITF with a phase-transition material results in a modulation of the sideband transmission while leaving the primary passband essentially unchanged. In such switchable ITFs, those sidebands can be re-engineered to act as secondary passbands. Therefore, such a design would allow independent control of transmission in different passbands via tuning the phase of the active material.

Here, we use a VO_2 film as the switchable layer. VO_2 features a dramatic change in the complex refractive index when the material undergoes an insulator-to-metal transition (IMT) at ∼70 °C (Figure 1d,e).[27] As shown in Figure 1c, once inserted into a bandpass filter, the insulator-phase VO_2 film has little effect on any transmission bands because of its low loss and deep-subwavelength thickness. In the metallic phase, the VO_2 film becomes lossy and can suppress the transmission at all wavelengths except the wavelength at which the electric field has a node at the VO_2 position. We designed two switchable ITFs: one that switches between double-passband and single-passband transmission states and a more complex design that switches between a narrow and a broadband transmission state. The former is primarily used to illustrate the design principle, and therefore it is only demonstrated by simulations. The latter was experimentally demonstrated as a proof-of-concept device for IR imaging enhancement.

To design a double-band transmission filter, we applied needle optimization methods[35,36] (in OpenFilters[37]) using two low-index materials (L), zinc sulfide (ZnS, n = 2.2) and barium fluoride (BaF_2, n = 1.42), and one high-index material (H), germanium (Ge, n = 4). We targeted a transmission spectrum with two high-transparency windows at 9 and 11 μm. The optimized structure, with the refractive index profile in Figure 2a, featured transmittance of ∼1 at both target wavelengths.

We found that at a depth of 5.2 μm (Figure 2a) $|E|$ featured a peak for λ = 9 μm and a node for λ = 11 μm. After we inserted a 50 nm VO_2 film at this position, the transmittance spectrum was largely unchanged for VO_2 in the insulating phase (OFF state). For VO_2 in the metallic phase (ON state), the transmittance at 9 μm was suppressed, while the transmittance at 11 μm remained mostly unaffected (Figure 2b). The refractive index of VO_2 used here was previously extracted by ellipsometry of a ∼ 100 nm VO_2 film synthesized using the sol−gel method on a silicon (Si) wafer.[27] A series of Lorentz oscillators were used to capture optical constants of the insulator-phase VO_2, and additional Drude terms were used to describe the contribution of the free carriers in the metallic phase. More characterization details are included in Supporting Information Section 1 and ref 27.

Then, via a similar procedure, we designed a broad-to-narrow bandpass ITF. We started with an all-dielectric stack with Ge (n = 4.0) as the high-index material and zinc selenide (ZnSe, n = 2.4) as the low-index material. We targeted high OFF-state transmittance (T_{OFF}) over 8−12 μm and narrowband ON-state transmittance (T_{ON}) at ∼9 μm. To minimize fabrication complexity, we limited the number of layers to 12

https://doi.org/10.1021/acs.nanolett.1c02296
Nano Lett. 2022, 22, 6−13

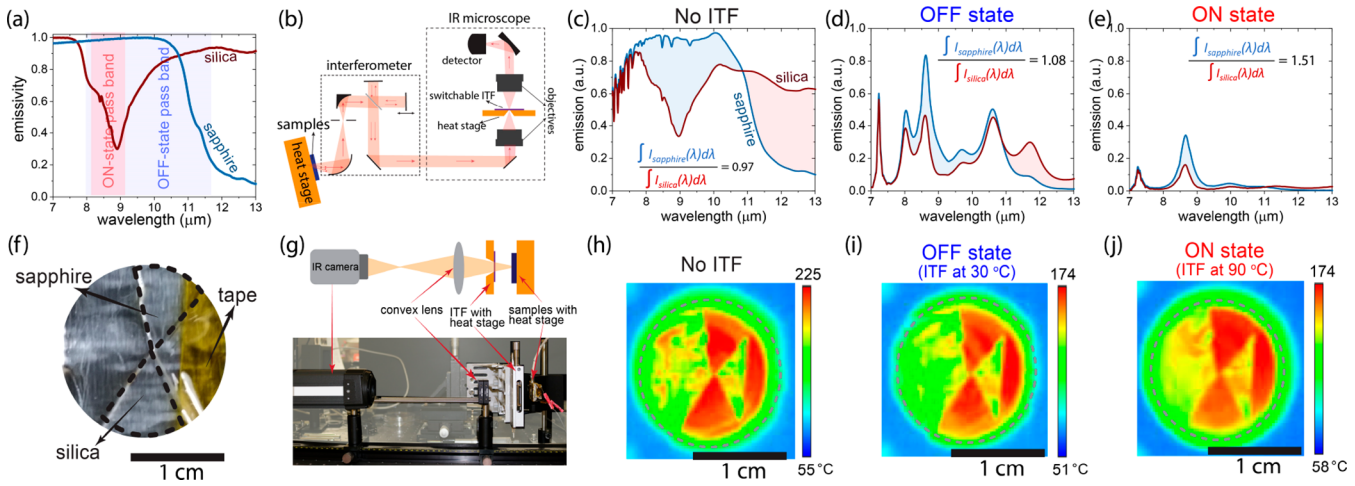

Figure 4. (a) Emissivities of the sapphire and silica wafer, measured by our FTIR spectrometer using Kirchhoff's law (i.e., emissivity = absorptance = 1 − reflectance, for an opaque wafer).[41] (b) Schematic of our thermal-emission measurements using the FTIR spectrometer. More details can be found in ref 40. (c−e) Measured thermally emitted signal from the sapphire and silica wafers when there was no ITF or with the ITF in its OFF state and ON state, respectively. (f) A visible photo of the sapphire and silica wafer pieces. (g) Our infrared imaging setup: the thermally emitted power from the sapphire and silica first went through the ITF and then was collected and reimaged by a convex lens to the object plane of an IR camera. (h−j) IR images of the heated sapphire and silica (at 280 °C) without the filter and for the ITF in its OFF state (25 °C) and ON (90 °C) state, respectively.

and the total thickness to 14.5 μm. We set the thickness of VO_2 in the design to be 72 nm, to match a VO_2 film we previously synthesized on a Si wafer (Supporting Information Section 1). In the optimization, we fixed the thickness of the Si to 1 μm to align with our fabricated device described in the next section. We set the optimization figure of merit as the product of the averaged OFF-state transmission (T_{OFF}) and the ratio between ON-state transmission (T_{ON}) within and outside of the passband at 8.8 μm:

$$\text{FOM} = T_{\text{OFF}}(8-12\ \mu\text{m})\frac{T_{\text{ON}}^{\max}(8.8\ \mu\text{m})}{T_{\text{ON}}(9.5-12\ \mu\text{m})}$$

The optimized structure (Figure 2c) features an OFF-state transmission band consisting of five adjoining bands with average transmittance >0.6 from 8 to 12 μm (Figure 2d). In the ON state, the peak transmittance reaches 0.5 at 8.8 μm with an out-of-band transmittance smaller than 0.1.

EXPERIMENTS

We fabricated the broad-to-narrow bandpass ITF based on the index profile in Figure 2c using the fabrication flow in Figure 3a. We used a 1-μm-thick Si (001) membrane supported by a frame (Norcada) as the substrate and oxidized it in a tube furnace at 850 °C for 5 h in air to promote VO_2 adhesion. The suspended membrane was wrinkled (Figure 3a−i). Our VO_2 films were produced by following Hanlon et al.[38] A vanadium-oxide sol was prepared by heating vanadium pentoxide (V_2O_5) powder (99.99% purity, AlphaAesar) in a ceramic crucible at 1100 °C until molten and then slowly pouring into water and filtering out the precipitates. The V_2O_5 solution was spin-coated onto the substrates (see details in Supporting Information Sections 1 and 3) and baked at 150 °C to evaporate the solvent. The membrane was then placed inside a tube furnace in a reducing atmosphere of 5% H_2 in Ar and annealed for 550 °C for 2 h to reduce the V_2O_5 film to VO_2 and promote crystal growth. Then, we deposited the alternating Ge−ZnSe layers on the top and bottom sides of the VO_2−Si membrane (Figure 3a-iii and iv) using electron-beam evaporation (implemented by Materion Corp.).

The OFF- and ON-state transmittance of the fabricated ITF was characterized using our FTIR spectrometer with a heat stage (Linkam FTIR 600) (see details in Supporting Information Section 2). The measurements are in qualitative agreement with our simulation. At 30 °C (filter in the OFF state), the device features an average transmittance of 0.34 across 8−12 μm. At 100 °C (filter in the ON state), our filter has a narrow passband at λ = 8.7 μm, with peak transmittance of 0.35, accompanied by low out-of-band transmittance (<0.03). The passband transmittance at 8.7 μm decreases by a factor of 2 as the device switches from the OFF state to the ON state, while the out-of-band transmittance decreases by an order of magnitude on average.

To understand the differences between our original simulations of the optimized structure and experiments, we performed several additional simulations. Three major factors were identified: (a) the thickness of VO_2 in our fabricated ITF is ∼130 nm, which is thicker than in the original design in Figure 2c,d. The thicker VO_2 results in a drop of the ON-state transmittance magnitude, as shown in Figure 3d (see more details in Supporting Information Section 3). (b) The drop of the OFF-state transmittance magnitude is likely due to the presence of metallic impurities in the insulator-phase VO_2, which is caused by the overreduction of V_2O_5, resulting in VO_x ($x < 2$)[29,39] which has more loss compared to pure insulating VO_2. Using an effective-medium calculation, we found that if we added ∼20% of the metal-phase domains to the OFF-state simulation (i.e., 20% of metallic phase + 80% of insulating phase rather than 100% of insulating phase in our original simulation) the magnitude drop of the simulated OFF-state transmittance matches the experiments (Figure 3c; see more details in Supporting Information Section 3). Note that the nontrivial OFF-state absorptance between 8 and 11 μm as shown in Figure S2c (Supporting Information Section 2) is evidence of the optical loss in the as-grown VO_2 film because pure insulating VO_2 has very little optical loss in this regime

https://doi.org/10.1021/acs.nanolett.1c02296
Nano Lett. 2022, 22, 6−13

(Figure 1e), and the other materials comprising the ITF are effectively lossless. (c) The transmittance peaks of the fabricated filter were blue-shifted by ∼0.1 μm compared to the simulation, which we attribute to thickness variations of the films due to fabrication errors. A 1.5% reduction in the thicknesses of all Ge and ZnSe layers captured this deviation very well, as shown in Figure 3c,d (Supporting Information Sections 3 and 4). Moreover, small differences in the refractive indices are expected among VO_2 films, though they were synthesized via very similar conditions.[27]

Despite these discrepancies, our fabricated ITF still features a good contrast in the transmittance bandwidth between the OFF and ON states and in principle can be used to enhance LWIR imaging. As a proof-of-concept demonstration, we used the switchable ITF to (1) modulate the thermal emission from two samples with different emissivity as measured using an FTIR spectrometer (top panel of Figure 4) and (2) modify IR imaging of these same samples using a commercial IR camera (bottom panel of Figure 4). The two samples we used are sapphire and silica wafers heated to 280 °C, which are nearly indistinguishable by thethe eye (Figure 4b) but have distinct LWIR emissivities. In our thermal emission measurements (Figure 4c), the emitted power from the samples went through the interferometer and then was directed to the microscope where our ITF was placed, and the filter state was controlled by a heat stage with a through-aperture hole. In this setup, though the ITF filter sometimes needed to work at high temperature (i.e., 90 °C for its ON state), its thermal-emission contribution was excluded from the measured signal because the ITF thermal emission was not modulated by the interferometer.

In Figure 4c−e, we show the raw measured thermal-emission spectrum (no calibration to account for the system response of the FTIR[40]) when no ITF is present (4c) and with the ITF in its OFF state (4d) and in its ON state (4e). Within the operational wavelength region of our switchable ITF, the emitted power from sapphire is larger than that of silica for shorter wavelengths but smaller for longer wavelengths. Therefore, the integrated powers of these two samples ($\int I(\lambda)\mathrm{d}\lambda$) are similar for the entire LWIR region when no ITF is present or when the ITF is in its OFF state. However, in the ON state of the ITF, the measured thermal power from the sapphire sample is significantly larger than that of silica (Figure 4e), indicating its potential for IR imaging enhancement.

Then, we incorporated our filter into an infrared imaging setup with an FLIR A325sc camera (Figure 4g). The thermally emitted light from the wafers went through the switchable ITF and a through-aperture hole on the heat stage, resulting in a limited field of view (the dashed circles in Figure 4h, i, and j). The transmitted power was collected using a convex lens and reimaged at the object plane of the camera. We set the camera emissivity to 0.95 (i.e., the emissivity the camera assumes when converting measured thermal-emission power into an apparent temperature) and temperature scale bar to autoscale mode for all the imaging, which is the default setting in the camera software. Then, we recorded images with no ITF (Figure 4h) and the ITF set to the OFF and ON states (Figure 4i,j), respectively. When there was no ITF, the silica appeared to be hotter than the sapphire by 5 °C (i.e., $\Delta T_{app} = T_{sapphire} - T_{silica} = -5$ °C). When the filter was used and set to its OFF state, ΔT_{app} became very close to zero. However, when the ITF was set to its ON state (i.e., 90 °C), the sapphire appeared to be hotter than silica (i.e., ΔT_{app} flipped its sign to +3 °C). These results qualitatively agree with our FTIR measurements in Figure 4c−e.

We note that we did not observe a large improvement in image contrast in Figure 4h−j as would be expected from our FTIR measurements in Figure 4c−e. The reason for this discrepancy is the significant background contributed by the thermal emission from the ITF itself because it has to be heated to 90 °C to be in the ON state and has significant emissivity (Supporting Information Section 2). The presence of the thermal background mostly cancels out the improvements to the image contrast obtained using the narrowband filter in the ON state of the ITF. In future realizations of switchable ITFs for image enhancement, the IMT temperature of VO_2 will need to be reduced, for example, using doping[42] or defect engineering.[43] We also note that the apparent temperatures interpreted by the camera in Figure 4h−j were very different from the actual temperature of the objects (∼280 °C), in part because we did not account for the true emissivities of the wafers and in part because the optical components between the objects and camera attenuated a significant amount of the emitted power from the objects.

DISCUSSION

Our multilayer geometry does not require nanopatterning, and thus this approach is more scalable and less expensive compared to the use of active metasurfaces.[44,45] Currently, the use of phase-change materials in the middle of thin-film stacks is uncommon (we note two demonstrations: ref 15 with GST and ref 46 with VO_2), likely because it has been challenging to integrate the active materials into dielectric stacks. For example, tunable near-IR Bragg filters have been demonstrated by introducing thin-film VO_2 as a defect layer into an alternating TiO_2/SiO_2 optical stack by sputtering all layers on a bulk quartz substrate.[46] However, for the LWIR regime, very few transparent materials are convenient substrates for the growth of VO_2.[47,48] Here, we demonstrated that a VO_2 film can be introduced into mid-IR-transparent stacks by synthesizing VO_2 on a thin Si membrane and then depositing thin films on both sides. Note that such VO_2-based filters can feature years-long lifetime, good reversibility, and reproducibility, if the fabrication is well controlled (see experimental evidence in Supporting Information Section 2). We also note that one could use the substrate transfer process[49,50] to fabricate the top and bottom thin-film coatings, which could be more suitable for fabricating over the centimeter scale.

The concept of switchable ITFs is applicable for any desired wavelength range so long as there are suitable active materials and low- and high-index dielectrics that can be deposited. Besides VO_2, many phase-transition materials have been explored for different wavelengths of interest, including Sb_2S_3[51] and 1T-TaS_2[52] for the visible, GST[15,25] for the near- and mid-infrared, and rare-earth perovskites[53] for the mid- and far-infrared. Moreover, we anticipate that more sophisticated optimization methods[54−56] can be used to significantly improve device figures of merit compared to those of our proof-of-concept device. Finally, we note that electrically triggering the IMT of VO_2[57,58] can be used to replace the thermal biasing for better integration with other components and to reduce the thermal background from the ITF itself.

https://doi.org/10.1021/acs.nanolett.1c02296
Nano Lett. 2022, 22, 6−13

CONCLUSION

We generalized the concept of an induced-transmission filter (ITF)—an old filter design that used a thin metal layer to suppress extraneous transmission bands in dielectric thin-film filters—by replacing the metal film with a tunable phase-transition layer and re-engineering the thicknesses of the surrounding high- and low-index dielectric layers. We designed active ITFs that can switch from one passband to many using vanadium dioxide (VO_2), a phase-transition material with large optical contrast between its two phases. By combining sol−gel synthesis of VO_2 on a thin membrane with electron-beam deposition of dielectric layers, we demonstrated an ITF that switches from a single narrow passband (at 8.8 μm) to a broadband transmission window (8−12 μm). Our active ITF can improve infrared imaging contrast under certain conditions. Moreover, our design and fabrication methods provide a platform for realizing tunable thin-film filters for wavelengths from the visible to the far-infrared with the proper choice of the active materials, enabling applications such as multispectral imaging[59] and imaging through obscurants.[60]

ASSOCIATED CONTENT

Supporting Information

The Supporting Information is available free of charge at https://pubs.acs.org/doi/10.1021/acs.nanolett.1c02296.

S1. Characterization of optical refractive index of VO_2. **S2**. Temperature-dependent FTIR measurements. **S3−4**. Analysis of differences between the simulation and experiment. **S5**. Incident-angle dependence of the switchable ITF (PDF)

AUTHOR INFORMATION

Corresponding Author

Mikhail A. Kats − *Department of Electrical and Engineering, University of Wisconsin—Madison, Madison, Wisconsin 53706, United States; Department of Materials Science and Engineering and Department of Physics, University of Wisconsin—Madison, Madison, Wisconsin 53706, United States;* orcid.org/0000-0003-4897-4720; Email: mkats@wisc.edu

Authors

Chenghao Wan − *Department of Electrical and Engineering, University of Wisconsin—Madison, Madison, Wisconsin 53706, United States; Department of Materials Science and Engineering, University of Wisconsin—Madison, Madison, Wisconsin 53706, United States;* orcid.org/0000-0002-4132-4779

David Woolf − *Physical Sciences, Inc., Andover, Massachusetts 01810, United States*

Colin M. Hessel − *Physical Sciences, Inc., Andover, Massachusetts 01810, United States*

Jad Salman − *Department of Electrical and Engineering, University of Wisconsin—Madison, Madison, Wisconsin 53706, United States*

Yuzhe Xiao − *Department of Electrical and Engineering, University of Wisconsin—Madison, Madison, Wisconsin 53706, United States;* orcid.org/0000-0002-0971-2480

Chunhui Yao − *Department of Electrical and Engineering, University of Wisconsin—Madison, Madison, Wisconsin 53706, United States*

Albert Wright − *Physical Sciences, Inc., Andover, Massachusetts 01810, United States*

Joel M. Hensley − *Physical Sciences, Inc., Andover, Massachusetts 01810, United States*

Complete contact information is available at: https://pubs.acs.org/10.1021/acs.nanolett.1c02296

Author Contributions

$^{\perp}$C.W. and D.W. contributed equally to this work. C.W., D.W., J.H., and M.K. conceived of the project and designed the experiments and simulations. D.W. and C.W. performed the simulations. D.W., C.H., and A.W. synthesized the VO_2 films. C.W., J.S., Y.X., and C.Y. built the experimental setup and carried out the experiments. All authors discussed the results and contributed to the writing of the manuscript. M.K. and J.H. supervised the project.

Notes

The authors declare no competing financial interest.

ACKNOWLEDGMENTS

This material is based on work supported by the Defense Advanced Research Projects Agency (DARPA) under Contract No. 140D6318C0013, and the paper was completed with support from the Office of Naval Research (ONR) under grant N00014-20-1-2297. The authors gratefully acknowledge use of facilities and instrumentation at the UW—Madison Wisconsin Centers for Nanoscale Technology (wcnt.wisc.edu) partially supported by the NSF through the University of Wisconsin Materials Research Science and Engineering Center (DMR-1720415).

REFERENCES

(1) Motorized Filter Wheels. https://www.thorlabs.com/newgrouppage9.cfm?objectgroup_id=988 (accessed Jul 22, 2020).

(2) *Ultra Narrowband Tunable Optical Filter*; TeraXion https://www.teraxion.com/en/products/optical-sensing/ultra-narrowband-tunable-optical-filter/ (accessed Jul 22, 2020).

(3) Haddad, E. I.; Zou, J.; Mohammad, N.; Kruzelecky, R.; Jamroz, W.; Szyszkowski, W.; Zhang, W. J. Analysis and Development of a Tunable Fiber Bragg Grating Filter Based on Axial Tension/Compression. *J. Light. Technol.* **2004**, *22* (8), 2001.

(4) Flanders, D. C. Tunable Fabry-Perot Filter. US6373632 B2, August 25, 2002.

(5) Barrios, C. A.; Almeida, V. R.; Panepucci, R. R.; Schmidt, B. S.; Lipson, M. Compact Silicon Tunable Fabry-Pérot Resonator With Low Power Consumption. *IEEE Photonics Technol. Lett.* **2004**, *16* (2), 506−508.

(6) Harris, S. E.; Wallace, R. W. Acousto-Optic Tunable Filter. *J. Opt. Soc. Am.* **1969**, *59* (6), 744.

(7) Tunable Filters (AOTF) https://gandh.com/product-categories/tunable-filters-aotf/ (accessed Jul 22, 2020).

(8) Liquid Crystal Tunable Bandpass Filters https://www.thorlabs.com/newgrouppage9.cfm?objectgroup_id=3488 (accessed Jul 22, 2020).

(9) Humar, M.; Ravnik, M.; Pajk, S.; Muševič, I. Electrically Tunable Liquid Crystal Optical Microresonators. *Nat. Photonics* **2009**, *3* (10), 595−600.

(10) Winzer, P. J.; Neilson, D. T.; Chraplyvy, A. R. Fiber-Optic Transmission and Networking: The Previous 20 and the next 20 Years [Invited]. *Opt. Express* **2018**, *26* (18), 24190.

(11) Favreau, P.; Hernandez, C.; Lindsey, A. S.; Alvarez, D. F.; Rich, T.; Prabhat, P.; Leavesley, S. J. Thin-Film Tunable Filters for Hyperspectral Fluorescence Microscopy. *J. Biomed. Opt.* **2014**, *19* (1), 011017.

(12) Gat, N. Imaging Spectroscopy Using Tunable Filters: A Review. In *Proceedings of SPIE*; Szu, H. H., Vetterli, M., Campbell, W. J., Buss, J. R., Eds.; SPIE, 2000; Vol. *4056*, pp 50−64. DOI: 10.1117/12.381686.
(13) Tao, J.; Yu, X.; Hu, B.; Dubrovkin, A.; Wang, Q. J. Graphene-Based Tunable Bragg Reflector with a Broad Bandwidth. *Conf. Lasers Electro-Optics Eur. - Technol. Dig.* **2014**, *2014* (2), 271−274.
(14) Wang, X.; Gong, Z.; Dong, K.; Lou, S.; Slack, J.; Anders, A.; Yao, J. Tunable Bragg Filters with a Phase Transition Material Defect Layer. *Opt. Express* **2016**, *24* (18), 20365.
(15) Williams, C.; Hong, N.; Julian, M.; Borg, S.; Kim, H. J. Tunable Mid-Wave Infrared Fabry-Perot Bandpass Filters Using Phase-Change GeSbTe. *Opt. Express* **2020**, *28* (7), 10583.
(16) Bhaskaran, H.; Youngblood, N.; He, Q.; Miao, X.; Cheng, Z.; Cheng, Z.; Cheng, Z.; Miao, X.; Bhaskaran, H.; Bhaskaran, H. Dynamically Tunable Transmissive Color Filters Using Ultra-Thin Phase Change Materials. *Opt. Express* **2020**, *28* (26), 39841−39849.
(17) Jadidi, M. M.; Sushkov, A. B.; Myers-Ward, R. L.; Boyd, A. K.; Daniels, K. M.; Gaskill, D. K.; Fuhrer, M. S.; Drew, H. D.; Murphy, T. E. Tunable Terahertz Hybrid Metal-Graphene Plasmons. *Nano Lett.* **2015**, *15* (10), 7099−7104.
(18) Julian, M. N.; Williams, C.; Borg, S.; Bartram, S.; Kim, H. J. Reversible Optical Tuning of GeSbTe Phase-Change Metasurface Spectral Filters for Mid-Wave Infrared Imaging. *Optica* **2020**, *7* (7), 746.
(19) Wan, C.; Zhang, Z.; Salman, J.; King, J.; Xiao, Y.; Yu, Z.; Shahsafi, A.; Wambold, R.; Ramanathan, S.; Kats, M. A. Ultrathin Broadband Reflective Optical Limiter. *Laser Photonics Rev.* **2021**, *15* (6), 2100001.
(20) Ozer, A.; Kocer, H.; Kurt, H. Tunable Optical Behavior of Infrared Filters with Phase Change Material. *J. Nanophotonics* **2018**, *12* (4), 046022.
(21) Garcia-Vidal, F. J.; Martin-Moreno, L.; Ebbesen, T. W.; Kuipers, L. Light Passing through Subwavelength Apertures. *Rev. Mod. Phys.* **2010**, *82* (1), 729−787.
(22) Wang, Q.; Rogers, E. T. F.; Gholipour, B.; Wang, C. M.; Yuan, G.; Teng, J.; Zheludev, N. I. Optically Reconfigurable Metasurfaces and Photonic Devices Based on Phase Change Materials. *Nat. Photonics* **2016**, *10* (1), 60−65.
(23) Siegel, J. F.; Dwyer, J. H.; Suresh, A.; Safron, N. S.; Fortman, M. A.; Wan, C.; Choi, J. W.; Wei, W.; Saraswat, V.; Behn, W.; Kats, M. A.; Arnold, M. S.; Gopalan, P.; Brar, V. W. Using Bottom-Up Lithography and Optical Nonlocality to Create Short-Wave Infrared Plasmonic Resonances in Graphene. *ACS Photonics* **2021**, *8* (5), 1277−1285.
(24) Shao, Z.; Cao, X.; Luo, H.; Jin, P. Recent Progress in the Phase-Transition Mechanism and Modulation of Vanadium Dioxide Materials. *NPG Asia Materials*; Nature Publishing Group; 2018; pp 581−605. DOI: 10.1038/s41427-018-0061-2.
(25) Zhang, Y.; Chou, J. B.; Li, J.; Li, H.; Du, Q.; Yadav, A.; Zhou, S.; Shalaginov, M. Y.; Fang, Z.; Zhong, H.; Roberts, C.; Robinson, P.; Bohlin, B.; Ríos, C.; Lin, H.; Kang, M.; Gu, T.; Warner, J.; Liberman, V.; Richardson, K.; Hu, J. Broadband Transparent Optical Phase Change Materials for High-Performance Nonvolatile Photonics. *Nat. Commun.* **2019**, *10* (1), 1−9.
(26) Gonçalves, P. A. D. Electronic and Optical Properties of Graphene. In *Plasmonics and light-matter interactions in two-dimensional materials and in metal nanostructures*; Springer: Cham, 2020; pp 51−70. DOI: 10.1007/978-3-030-38291-9_3.
(27) Wan, C.; Zhang, Z.; Woolf, D.; Hessel, C. M.; Rensberg, J.; Hensley, J. M.; Xiao, Y.; Shahsafi, A.; Salman, J.; Richter, S.; Sun, Y.; Qazilbash, M. M.; Schmidt-Grund, R.; Ronning, C.; Ramanathan, S.; Kats, M. A. On the Optical Properties of Thin-Film Vanadium Dioxide from the Visible to the Far Infrared. *Ann. Phys.* **2019**, *531* (10), 1900188.
(28) Nag, J.; Haglund, R. F., Jr Synthesis of Vanadium Dioxide Thin Films and Nanoparticles. *J. Phys.: Condens. Matter* **2008**, *20* (26), 264016.
(29) Zhang, Z.; Zuo, F.; Wan, C.; Dutta, A.; Kim, J.; Rensberg, J.; Nawrodt, R.; Park, H. H.; Larrabee, T. J.; Guan, X.; Zhou, Y.; Prokes, S. M.; Ronning, C.; Shalaev, V. M.; Boltasseva, A.; Kats, M. A.; Ramanathan, S. Evolution of Metallicity in Vanadium Dioxide by Creation of Oxygen Vacancies. *Phys. Rev. Appl.* **2017**, *7* (3), 034008.
(30) Devthade, V.; Lee, S. Synthesis of Vanadium Dioxide Thin Films and Nanostructures. *J. Appl. Phys.* **2020**, *128* (23), 231101.
(31) Cui, Y.; Ramanathan, S. Substrate Effects on Metal-Insulator Transition Characteristics of Rf-Sputtered Epitaxial VO 2 Thin Films. *J. Vac. Sci. Technol. A Vacuum, Surfaces, Film.* **2011**, *29* (4), 041502.
(32) Berning, P. H.; Turner, A. F. Induced Transmission in Absorbing Films Applied to Band Pass Filter Design. *J. Opt. Soc. Am.* **1957**, *47* (3), 230.
(33) Holloway, R. J.; Lissberger, P. H. The Design and Preparation of Induced Transmission Filters. *Appl. Opt.* **1969**, *8* (3), 653.
(34) Macleod, H. A. *Thin-Film Optical Filters*; CRC Press/Taylor & Francis, 2010; pp 299−399.
(35) Tikhonravov, A. V.; Trubetskov, M. K.; DeBell, G. W. Optical Coating Design Approaches Based on the Needle Optimization Technique. *Appl. Opt.* **2007**, *46* (5), 704−710.
(36) Tikhonravov, A. V.; Trubetskov, M. K. Modern Design Tools and a New Paradigm in Optical Coating Design. *Appl. Opt.* **2012**, *51* (30), 7319.
(37) Larouche, S.; Martinu, L. OpenFilters: Open-Source Software for the Design, Optimization, and Synthesis of Optical Filters. *Appl. Opt.* **2008**, *47* (13), C219−C230.
(38) Hanlon, T. J.; Walker, R. E.; Coath, J. A.; Richardson, M. A. Comparison between Vanadium Dioxide Coatings on Glass Produced by Sputtering, Alkoxide and Aqueous Sol-Gel Methods. *Thin Solid Films* **2002**, *405* (1−2), 234−237.
(39) Schwingenschlögl, U.; Eyert, V. The Vanadium Magnéli Phases VnO2n-1. *Ann. Phys.* **2004**, *13* (9), 475−510.
(40) Xiao, Y.; Wan, C.; Shahsafi, A.; Salman, J.; Yu, Z.; Wambold, R.; Mei, H.; Perez, B. E. R.; Derdeyn, W.; Yao, C.; Kats, M. A. Precision Measurements of Temperature-Dependent and Non-equilibrium Thermal Emitters. *Laser Photonics Rev.* **2020**, *14* (8), 1900443.
(41) Yao, C.; Mei, H.; Xiao, Y.; Shahsafi, A.; Derdeyn, W.; King, J. L.; Wan, C.; Scarlat, R. O.; Anderson, M. H.; Kats, M. A. Correcting Thermal-Emission-Induced Detector Saturation in Infrared Spectroscopy. *arXiv preprint.* **2020**, arXiv:2012.14987 (accessed Jan 31, 2021).
(42) Manning, T. D.; Parkin, I. P.; Pemble, M. E.; Sheel, D.; Vernardou, D. Intelligent Window Coatings: Atmospheric Pressure Chemical Vapor Deposition of Tungsten-Doped Vanadium Dioxide. *Chem. Mater.* **2004**, *16* (4), 744−749.
(43) Rensberg, J.; Zhang, S.; Zhou, Y.; McLeod, A. S.; Schwarz, C.; Goldflam, M.; Liu, M.; Kerbusch, J.; Nawrodt, R.; Ramanathan, S.; et al. Active Optical Metasurfaces Based on Defect-Engineered Phase-Transition Materials. *Nano Lett.* **2016**, *16* (2), 1050−1055.
(44) Shaltout, A. M.; Kildishev, A. V.; Shalaev, V. M. Evolution of Photonic Metasurfaces: From Static to Dynamic. *J. Opt. Soc. Am. B* **2016**, *33* (3), 501.
(45) He, Q.; Sun, S.; Zhou, L. Tunable/Reconfigurable Metasurfaces: Physics and Applications. *Research* **2019**, *2019*, 1−16.
(46) Wang, X.; Gong, Z.; Dong, K.; Lou, S.; Slack, J.; Anders, A.; Yao, J. Tunable Bragg Filters with a Phase Transition Material Defect Layer. *Opt. Express* **2016**, *24* (18), 20365.
(47) Kovács, G. J.; Bürger, D.; Skorupa, I.; Reuther, H.; Heller, R.; Schmidt, H. Effect of the Substrate on the Insulator-Metal Transition of Vanadium Dioxide Films. *J. Appl. Phys.* **2011**, *109* (6), 063708.
(48) Marvel, R. E.; Harl, R. R.; Craciun, V.; Rogers, B. R.; Haglund, R. F. Influence of Deposition Process and Substrate on the Phase Transition of Vanadium Dioxide Thin Films. *Acta Mater.* **2015**, *91*, 217−226.
(49) Arscott, S.; Mounaix, P.; Lippens, D. Substrate Transfer Process for InP-Based Heterostructure Barrier Varactor Devices. *J. Vac. Sci. Technol. B Microelectron. Nanom. Struct.* **2000**, *18* (1), 150.
(50) Lee, K. H.; Bao, S.; Zhang, L.; Kohen, D.; Fitzgerald, E.; Tan, C. S. Integration of GaAs, GaN, and Si-CMOS on a Common 200mm

Si Substrate through Multilayer Transfer Process. *Appl. Phys. Express* **2016**, *9* (8), 086501.
(51) Dong, W.; Liu, H.; Behera, J. K.; Lu, L.; Ng, R. J. H.; Sreekanth, K. V.; Zhou, X.; Yang, J. K. W.; Simpson, R. E. Wide Bandgap Phase Change Material Tuned Visible Photonics. *Adv. Funct. Mater.* **2019**, *29* (6), 1806181.
(52) Li, W.; Naik, G. V. In-Plane Electrical Bias Tunable Optical Properties of 1T-TaS 2 [Invited]. *Opt. Mater. Express* **2019**, *9* (2), 497.
(53) Li, Z.; Zhou, Y.; Qi, H.; Pan, Q.; Zhang, Z.; Shi, N. N.; Lu, M.; Stein, A.; Li, C. Y.; Ramanathan, S.; Yu, N. Correlated Perovskites as a New Platform for Super-Broadband-Tunable Photonics. *Adv. Mater.* **2016**, *28* (41), 9117−9125.
(54) Liu, D.; Tan, Y.; Khoram, E.; Yu, Z. Training Deep Neural Networks for the Inverse Design of Nanophotonic Structures. *ACS Photonics* **2018**, *5* (4), 1365−1369.
(55) Unni, R.; Yao, K.; Zheng, Y. Deep Convolutional Mixture Density Network for Inverse Design of Layered Photonic Structures. *ACS Photonics* **2020**, *7* (10), 2703−2712.
(56) Azunre, P.; Jean, J.; Rotschild, C.; Bulovic, V.; Johnson, S. G.; Baldo, M. A. Guaranteed Global Optimization of Thin-Film Optical Systems. *New J. Phys.* **2019**, *21* (7), 073050.
(57) Yang, Z.; Ko, C.; Ramanathan, S. Oxide Electronics Utilizing Ultrafast Metal-Insulator Transitions. *Annu. Rev. Mater. Res.* **2011**, *41* (1), 337−367.
(58) Chen, S.; Wang, Z.; Ren, H.; Chen, Y.; Yan, W.; Wang, C.; Li, B.; Jiang, J.; Zou, C. Gate-Controlled VO 2 Phase Transition for High-Performance Smart Windows. *Sci. Adv.* **2019**, *5* (3), No. eaav6815.
(59) Tittl, A.; Michel, A.-K. U.; Schäferling, M.; Yin, X.; Gholipour, B.; Cui, L.; Wuttig, M.; Taubner, T.; Neubrech, F.; Giessen, H. A Switchable Mid-Infrared Plasmonic Perfect Absorber with Multispectral Thermal Imaging Capability. *Adv. Mater.* **2015**, *27* (31), 4597−4603.
(60) Steinvall, O. K.; Olsson, H.; Bolander, G.; Groenwall, C. A.; Letalick, D. Gated Viewing for Target Detection and Target Recognition. In *Laser Radar Technology and Applications IV*; Kamerman, G. W., Werner, C., Eds.; SPIE, 1999; Vol. *3707*, p 432. DOI: 10.1117/12.351364.

https://doi.org/10.1021/acs.nanolett.1c02296
Nano Lett. 2022, 22, 6−13